Calibration of a Calorimeter for Thermal Resistance Measurements of Advanced Insulation Panels

by

Michael W. Ellis
Virginia Polytechnic Institute and State University
Blacksburg, VA

And

A. Hunter Fanney and Mark W. Davis
Building and Fire Research Laboratory
National Institute of Standards and Technology
Gaithersburg, MD 20899 USA

Reprinted from HVAC & R Research, Vol. 6, No. 3, July 2000

NIST
National Institute of Standards and Technology
Technology Administration, U.S. Department of Commerce

Calibration of a Calorimeter for Thermal Resistance Measurements of Advanced Insulation Panels

M.W. Ellis, Ph.D., P.E.
Member ASHRAE

A.H. Fanney, Ph.D.
Member ASHRAE

M.W. Davis

Insulation technologies are being developed to reduce the energy consumption associated with refrigerators, freezers, and the transport of refrigerated products. Among the insulation concepts being explored are powder, foam, glass-fiber-filled evacuated panels, and low-conductivity gas-filled panels. These advanced insulation panels offer the potential for significant reductions in energy consumption and greater flexibility in product design. Unfortunately, the equipment used to determine the thermal resistance of traditional building insulation materials is not well suited for measuring the thermal resistance of advanced insulation panels.

This paper describes a calorimetric apparatus to measure the thermal resistance of advanced insulation materials. It presents the procedures used to determine the thermal resistance of advanced insulation panels, and compares the calorimetric results to measurements from the guarded hot plate for extruded polystyrene specimens. The measurements agree to within 3% over a mean temperature range of 280 to 295 K.

INTRODUCTION

Thermal insulation systems are under development that possess superior insulating capabilities in comparison to commonly used building insulation materials (NIBS 1995). Among the advanced insulation systems currently being explored are compact vacuum insulation panels, powder-filled or foam-filled panels, and gas-filled panels.

Compact vacuum insulation panels are comprised of rigid metallic walls separated by spacers to form an evacuated space. Radiation transfer within the enclosure is minimized through the use of low-emissivity coatings. Powder-filled or foam-filled panels use a powder or open-cell foam encapsulated in a gas barrier that prevents air diffusion into the vacuum. The gas diffusion barrier may consist of various polymers, metallic materials, or a combination. Gas-filled panels combine low-emissivity surfaces and multiple, low-conductivity gas-filled cavities to minimize radiation, convection, and conduction. Gases that have been used to date include argon, krypton, and xenon (Griffith and Arasteh 1992).

Measurement techniques and apparatuses are needed that allow an accurate determination of the thermal resistance of advanced insulation systems. Advanced insulation systems have one or more characteristics that preclude the use of guarded hot plates and heat flow meter apparatuses, the equipment used to measure the thermal conductance of traditional building insulation materials. For example, guarded hot plate and heat flow meter apparatuses are designed to measure the thermal conductivity of isotropic, homogenous test samples that are representative of full assemblies. Both apparatuses are designed in a manner that attempts to limit to one direction the flow

M.W. Ellis is a professor in the Department of Mechanical Engineering, Virginia Polytechnic Institute and State University, Blacksburg, VA. **A.H. Fanney** is ____ in the Building Environment Division of the National Institute of Standards and Technology, Gaithersburg, MD. **M.W. Davis** was a graduate student??? in the Department of Mechanical Engineering, Virginia Polytechnic Institute and State University.

of heat. However, the heat transfer through advanced insulation systems is not limited to one direction due to the barrier materials used in their construction (Glicksman 1995; Caps 1997).

In addition, ASTM *Test Method* C 177, which prescribes the standard test method for guarded hot plate apparatuses, states that testing of inhomogeneous materials can result in significant measurement errors (ASTM 1997). Advanced insulation materials are typically constructed of two or more materials. ASTM *Test Method* C 177 further specifies that the surfaces of the test specimens be flat and parallel to minimize surface contact resistance. Compact vacuum insulation panels typically exhibit surface depressions between the spacers that are used to hold the barrier apart under the atmospheric load. ASTM *Test Method* C 518, which applies to heat flow meter apparatuses, states that special care should be taken for specimens exhibiting appreciable inhomogeneities, rigidity, or especially high or low resistance to heat (ASTM 1997). Advanced insulation systems are designed to have high resistance to heat flow, are inhomogeneous, and, in the case of metal clad panels, are rigid in construction.

In order to avoid the limitations of these measurement techniques, a calorimetric technique has been developed to permit the measurement of the thermal performance of advanced insulation systems (Fanney et al. 1995). This paper describes the calorimetric apparatus and the procedures used at NIST to determine the thermal resistance of advanced insulation panels. The flanking losses associated with the calorimeter are quantified using finite element analysis. Comparisons are made between measurements conducted on extruded polystyrene specimens using the calorimetric apparatus and the NIST 1-meter guarded hot plate.

EXPERIMENTAL APPARATUS

A calorimetric apparatus, Figure 1, was developed to measure the thermal performance of advanced insulation panels. The apparatus consisted of a climatic chamber, a metering chamber, masks, a precision power supply, instrumentation, and a personal computer.

The climatic chamber, constructed by removing the doors and installing an air plenum within a commercial freezer, maintained the air temperature adjacent to the rear surface of the insulating panel below ambient. A turning vane and tangential fan at the entrance and exit of the plenum, respectively, provided an air velocity of approximately 3.52 m/s across the rear surface of the panel. Sixteen type-T thermocouples were used to measure the air temperature within the plenum. The desired air temperature was maintained by continuously running the compressor of the freezer and supplying power to a resistance heater located downstream of the evaporator coil. A vertical temperature gradient of approximately 0.5 K existed within the air plenum.

The metering chamber was constructed of extruded polystyrene and can accommodate panels up to 0.914 m by 0.915 m wide. A neoprene gasket located between the metering chamber and mask provided an air seal between the interior of the metering chamber and the surrounding air. The gasket was compressed by means of nylon straps placed around the metering chamber. A 32-junction thermopile provided a signal proportional to the temperature differential between the interior and exterior surfaces of the rear wall of the calorimeter. The signal was fed to a computer-based data acquisition system that incorporated a proportional-integral-derivative controller algorithm. The output of the controller was fed to a precision power supply that supplied power to a 27-gage nickel chromium heater within the calorimeter. The power was continuously adjusted such that the air temperature within the metering chamber was maintained at a level approximately equivalent to laboratory ambient. Sixteen thermocouples were used to measure the air temperature within the metering chamber. Any air movement within the metering chamber was a result of natural convection. A 3.0 K vertical temperature gradient typically existed within the metering chamber.

The test specimen was centrally located in a nominal 50 mm extruded polystyrene mask. The mask was used to fill the void between the perimeter of the calorimeter box and the insulating

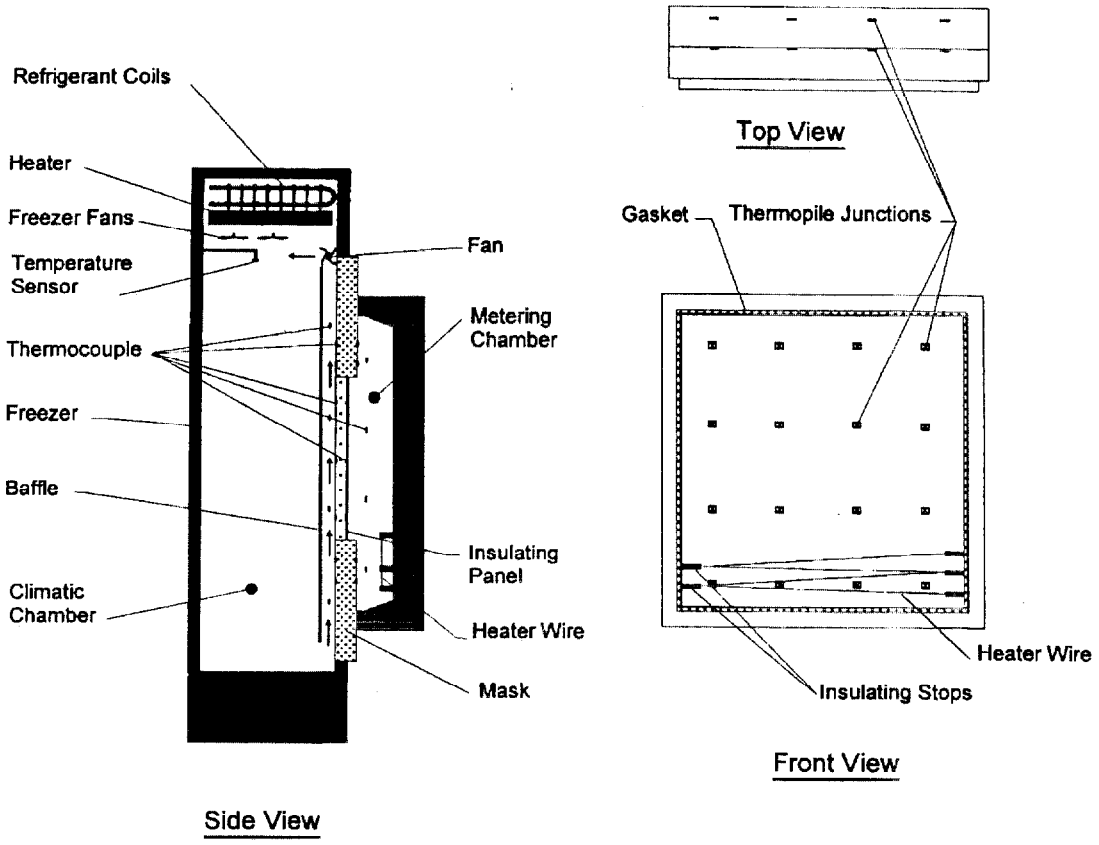

Figure 1. Calorimetric apparatus

panel, allowing panels of various sizes to be tested. The thermal conductivity of extruded polystyrene increases with time as a result of the diffusion of air into and blowing agent out of the material (Brandreth 1991). In an attempt to minimize this "aging" effect, the extruded polystyrene mask material was purchased approximately 16 months before use in the calorimeter. The thermal conductivity was measured every two weeks using a heat flow meter apparatus (ASTM C 518) until the rate of thermal conductivity change was negligible. The NIST 1-meter guarded hot plate was subsequently used to measure the thermal conductivity of the material as a function of mean temperature.

In addition to the thermocouples used to measure the air temperatures within the calorimeter box and air plenum, the apparatus can monitor up to a total of 72 surface and/or panel thermocouples. All transducer measurements, except power measurements, were fed to a data acquisition system interfaced to a personal computer. The personal computer converted the thermocouple and thermopile outputs into engineering units, graphically displayed the acquired data, and recorded the resulting data. The power supply, connected to the electrical heater of the calorimeter, was controlled and monitored by the personal computer using an IEEE-488 digital interface.

The average air temperature adjacent to the panel in the metering chamber was measured using 16 uniformly spaced thermocouples. An identical thermocouple grid located in the air plenum behind the panel was used to determine the average air temperature adjacent to the panel in the climatic chamber. Panel surface temperatures were determined using thermocouples attached to the insulating panel. A maximum of 18 thermocouples may be monitored on each side of the panel. In accordance with ASTM C 976, thermocouple placement is dependent upon the type of panel

being evaluated (ASTM 1997). For homogenous panels, the thermocouples were positioned uniformly and symmetrically such that all thermocouples monitored equal areas. During evaluation of inhomogeneous panels, such as metal-clad vacuum insulation panels, the surface temperature of the panel was not uniform. For inhomogeneous panels, the thermal resistance of the panel was determined by subtracting the resistance attributable to the surface conductance for each side of the panel from the overall thermal resistance determined from the heat transfer rate and the air temperatures in the environmental and metering chambers. For consistency, the thermal resistance measurements presented in this paper are determined in the same manner.

ANALYSIS

Thermal Resistance of Insulating Panel

The thermal resistance of an insulating panel is based on the heat transfer from the hot to the cold side of the panel, the associated temperatures, and the panel size. Figure 2 illustrates the ideal arrangement for measuring heat transfer through the panel. In this ideal arrangement, the heat flux is nonuniform due to the inhomogeneous construction of the panel, but there is no heat transfer from the ends of the panel. Figure 3 illustrates the actual heat transfer paths in the calorimeter assembly. In the actual case, heat may transferred not only through the insulating panel, but also through the walls of the calorimeter, axially through the mask, and laterally into the mask. In addition, the heat transfer in the vicinity of the boundary between the mask and the panel is enhanced due to the interaction between these components. In the measurement technique described here, heat transfer through the calorimeter walls is minimized by control of the calorimeter temperature, and heat transfer through the mask is evaluated using finite element techniques. The interaction between the mask and the insulating panel is described in an earlier publication (Fanney et al. 1995).

An energy balance on the calorimeter results in the following equation:

$$Q_{HTR} = Q_{IP} + Q_M + Q_W + Q_F \tag{1}$$

where

Q_{HTR} power supplied to the calorimeter's electric heater, W
Q_{IP} axial heat transfer through the insulating panel, W
Q_M axial heat transfer through the surrounding mask, W
Q_W heat transfer through the metering chamber's walls, W
Q_F heat transfer laterally through the mask at the perimeter of the metering chamber (referred to as *flanking loss*), W

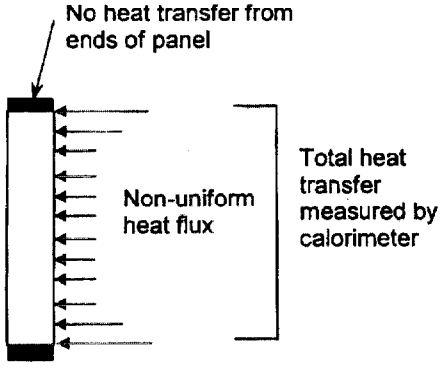

Figure 2. Ideal heat transfer path

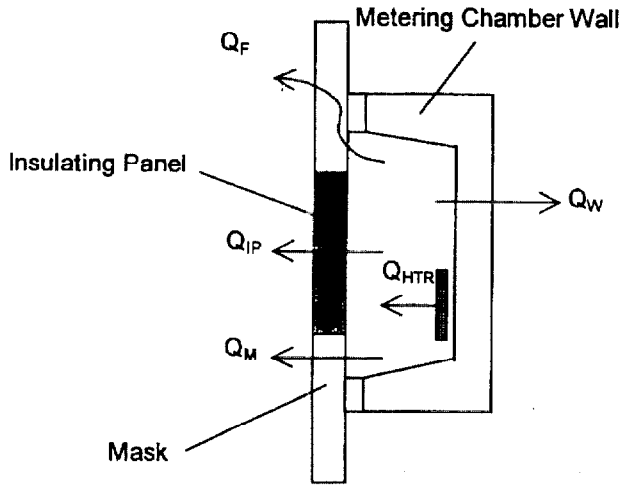

Figure 3. Heat transfer paths in calorimeter assembly

The various heat flows are illustrated in Figure 3.

Referring to Equation (1), the power supplied to the heater Q_{HTR} can be determined from measured quantities, the heat transfer through the metering chamber walls Q_W can be reduced to a negligible value by proper control of the calorimeter, and values for the mask heat transfer Q_M and flanking loss Q_F can be determined as described in the following section. With these values known, Equation (1) can be solved for the heat transfer through the insulating panel. The heat transfer through the insulating panel can then be used to calculate the thermal resistance of the insulating panel.

Tests conducted during the design of the calorimeter revealed that Q_W is less than 0.5% of Q_{HTR}. It was also determined that the rear wall of the metering chamber was responsible for 80% of Q_W. Based on these findings, a thermopile was installed across the rear wall of the metering chamber. By controlling the temperature in the metering chamber so that the temperature difference sensed by the thermopile approaches zero, the wall heat transfer Q_W can be reduced to a negligible value.

With Q_W neglected, the heat flow through the insulated specimen and the surrounding mask is given by

$$Q_{IP} + Q_M = Q_{HTR} - Q_F \tag{2}$$

The heat flow through the insulation and surrounding mask may also be expressed as

$$Q_{IP} + Q_M = Q'_{IP} + Q'_M + Q_D \tag{3}$$

where

Q'_{IP} axial heat transfer that would occur through the insulation panel if the boundary adjacent to the mask were adiabatic, W

Q'_M axial heat transfer which would occur through the mask if the boundary adjacent to the insulation panel were adiabatic, W

Q_D difference between the heat transfer through the combined insulation panel and surrounding mask assembly and the sum of the heat transfer through each individual component if the common boundary were adiabatic, W

In this expression, Q_D accounts for the two-dimensional effect at the mask-panel interface due to the unequal conductances of the two components.

Combining Equations (2) and (3) and rearranging yields

$$Q'_{IP} = Q_{HTR} - Q_F - Q'_M - Q_D \tag{4}$$

The methodology used to quantify Q_D and representative results for selected advanced insulation panels are presented in an earlier publication (Fanney et al. 1995). Flanking loss Q_F and Q'_M are computed in accordance with the procedures outlined in the following section.

Having determined the heat transfer Q'_{IP} that would occur through the insulation panel if the boundary with the mask were adiabatic, the thermal resistance of the insulating panel can be determined from

$$R_{IP} = \frac{A_{IP}(T_M - T_C)}{Q'_{IP}} - \frac{1}{h_M} - \frac{1}{h_C} \tag{5}$$

where

R_{IP} thermal resistance of the panel, $m^2 \cdot K/W$
A_{IP} insulating panel's area, m^2
T_M average temperature of the air adjacent to the panel in the metering chamber, K
T_C average temperature of the air adjacent to the panel in the environmental chamber, K
h_M surface conductance for the side of the panel exposed to the metering chamber, $W/m^2 \cdot K$
h_C surface conductance for the side of the panel exposed to the climatic chamber, $W/m^2 \cdot K$

The panel's surface conductances are determined using the following expressions:

$$h_M = \frac{Q'_{IP}}{A_{IP}(T_M - T_{SM})} \tag{6}$$

$$h_C = \frac{Q'_{IP}}{A_{IP}(T_C - T_{SC})} \tag{7}$$

where

T_{SM} average temperature of the panel surface exposed to the metering chamber, K
T_{SC} average temperature of the panel surface exposed to the environmental chamber, K

The average panel surface temperatures are determined using thermocouples attached to the insulating panel. A maximum of 18 thermocouples may be monitored on each side of the panel. For homogenous panels, the thermocouples are positioned uniformly and symmetrically such that all thermocouples monitor equal areas. The average air temperature adjacent to the panel in the metering chamber is measured using 16 uniformly spaced thermocouples. An identical thermocouple grid, located in the air plenum behind the panel, is used to determine the average air temperature adjacent to the panel in the environmental chamber. The surface conductances for the inhomogeneous panels are assumed to be the same as those determined for the homogeneous panels.

Flanking Loss

The flanking loss Q_F for a calorimeter refers to lateral heat transfer through the sample mask at the perimeter of the calorimeter (Figure 3). Flanking loss is dependent on the materials and

geometry of the calorimeter, the thickness and thermal conductivity of the mask and panel, and the boundary conditions to which the metering chamber and mask/panel assembly are subjected.

In order to quantify the flanking loss, one quadrant of the metering chamber, mask, and insulating panel (Figure 4a) was modelled using a commercially available finite element software package. The calorimeter components were divided into volumes suitable for meshing with 8-node solid elements. The finite element software was then applied to generate the mesh illustrated in Figure 4b and to solve the model based on the boundary conditions. In order to evaluate the adequacy of the mesh, the solution error resulting from the indicated mesh spacing was estimated using a technique implemented in the finite element software. With this technique, an error in the energy balance is calculated based on the discontinuity of the heat transfer between elements. For the indicated mesh, the error was estimated to be 1.3%.

Initially a continuous mask was modelled in lieu of a panel/mask assembly. This simplification eliminated the heat transfer Q_{IP} through the panel and the panel/mask interaction effect Q_D. Further, it was assumed that no heat transfer occurred through the metering chamber walls. Thus, Equation (4) is reduced to

$$Q_F = Q_{HTR} - Q'_M \tag{8}$$

An energy balance on the calorimeter cavity quadrant requires that in order to maintain a constant temperature, the energy added by the heater must equal the heat transfer through the interior surface areas of the calorimeter cavity including the mask:

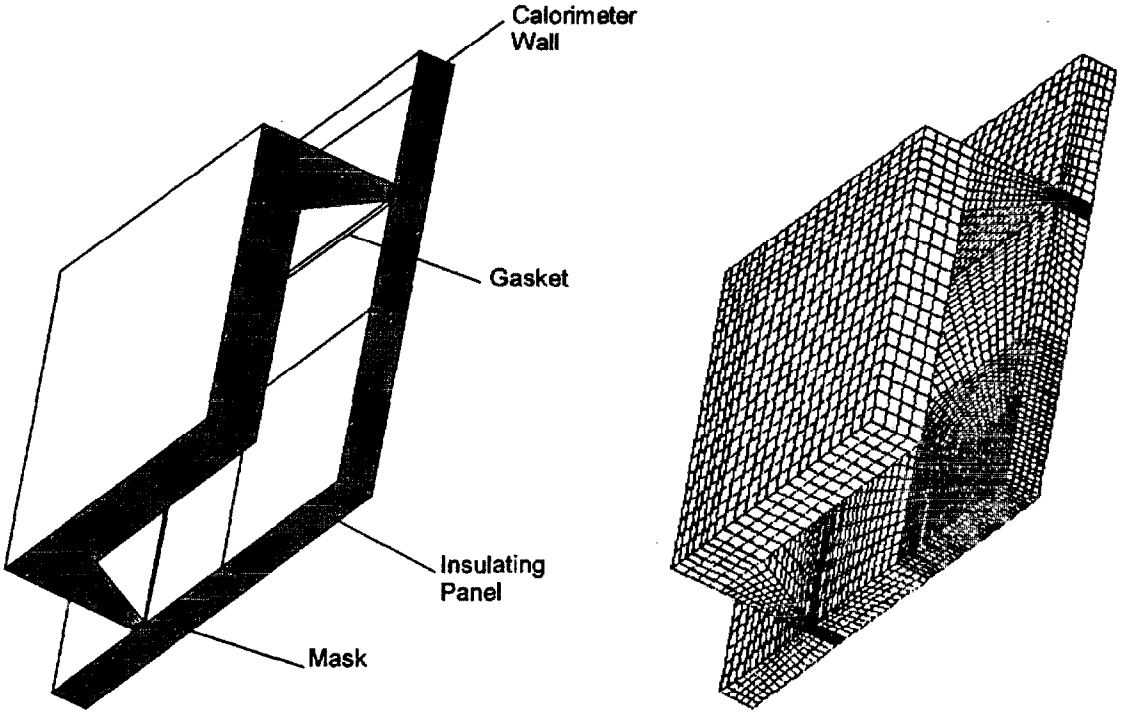

(a) Calorimeter Model (b) Finite Element Mesh

Figure 4. Calorimeter model and finite element mesh

$$Q_{HTR} = \sum_{\substack{\text{interior} \\ \text{surfaces of} \\ \text{calorimeter} \\ \text{cavity}}} Q_j \tag{9}$$

where Q_j is the heat transfer through element j on the interior surface of the calorimeter cavity.

The solution of the finite element model determines the heat transfer Q_j through the elements in each of the surface regions.

The axial heat transfer Q'_M through the mask can be determined from

$$Q'_M = \frac{A_M(T_M - T_C)}{\frac{L_M}{K_M} + \frac{1}{h_C} + \frac{1}{h_M}} \tag{10}$$

where

A_M area of the mask, m^2
L_M mask's thickness, m
k_M thermal conductivity of the mask material, W/m·K

The boundary conditions used in the finite element model and Equation (10) were set equivalent to measured values. On surfaces within the climatic chamber, these boundary conditions consist of a surface conductance of approximately 13.5 $W/m^2 \cdot K$ and an air temperature T_C within the climatic chamber. Boundary conditions within the metering chamber consist of free convection with a surface conductance of approximately 7.8 $W/m^2 \cdot K$ and an air temperature T_M corresponding to that of the metering chamber.

In order to determine the extent to which the insulating panel affects the flanking loss, the finite element model was revised to include a theoretical insulating panel. The thermal conductivity k_{ip} of the theoretical insulating panel was chosen to be substantially different from that of the mask. The flanking loss for this case can be calculated by combining Equations (2) and (9) and neglecting the wall heat transfer to yield

$$Q_F = \sum_{\substack{\text{interior} \\ \text{surfaces of} \\ \text{calorimeter} \\ \text{cavity}}} Q_j - Q_{IP} - Q_M \tag{11}$$

where Q_{IP} and Q_M are determined from a finite element model. The dimensions of the theoretical insulating panel and its thermal conductivity were varied to determine the influence of the panel on the flanking loss.

RESULTS

Figure 5 illustrates the flanking loss expressed as a function of the difference between the metering and climatic chamber air temperatures for the specified calorimeter, specified mask material and thickness, and metering chamber temperature T_M. As this figure indicates, the flanking loss increases linearly with temperature difference. For the specified calorimeter and a 50 mm thick continuous extruded polystyrene mask, a linear regression indicates that the flanking loss is given by

$$Q_F = C_F(T_M - T_E) \tag{12}$$

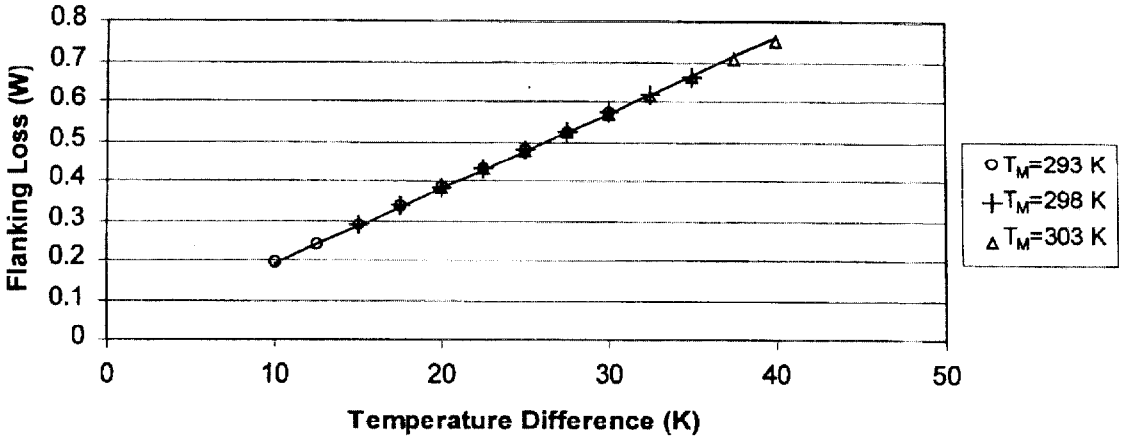

Figure 5. Calculated effect of temperature on flanking loss

where the flanking loss coefficient C_F is 0.019 W/K. Flanking loss accounts for approximately 4.5% of the total energy supplied by the heater.

The relationship between flanking loss and temperature difference illustrated in Figure 5 was developed for a continuous mask. In order to evaluate the influence of an insulating panel on the flanking loss, the finite element model was modified to include an insulating panel. A parametric study was conducted in which the length and width of the panel were varied from 15% to 95% of the inside dimensions of the calorimeter and the thermal conductivity of the panel was varied from 20% to 160% of the mask conductivity. Throughout this range of parameters, the flanking loss was within 5% of the flanking loss determined for the case of a continuous mask. These small variations in flanking loss affect the overall calorimeter energy balance by less than 0.25%. Therefore, the flanking loss predicted by Equation (12) is an adequate approximation to the flanking loss even for the case in which an insulating panel is installed in the mask.

Comparison of Calorimeter Results to Guarded Hot Plate Results

Tests were conducted to compare thermal resistance measurements made using the calorimeter to measurements made using the NIST 1-meter guarded hot plate, an apparatus that conforms to ASTM *Test Method* C 177. As previously noted, guarded hot plate apparatuses are not well suited for measuring the thermal resistance of advanced insulation panels. In order to compare measurements between the calorimeter apparatus and the NIST 1-meter guarded hot plate, a continuous sheet of extruded polystyrene was used in lieu of an advanced insulation panel/mask assembly. In this limiting case, Q_D and Q'_{IP} are zero, and Equation (4) simplifies to

$$Q'_M = Q_{HTR} + Q_F \tag{13}$$

The power supplied to the calorimeter's heater was determined using measured values. The flanking loss was determined using Equation (12). To minimize measured differences due to specimen variability, the guarded hot plate specimens were fabricated from the material used in the calorimeter apparatus. The resulting measurements are shown in Figure 6 as a function of mean specimen temperature.

The calorimeter results, uncorrected for flanking loss, are depicted as open squares in Figure 6. The solid triangles represent the calorimeter results after flanking loss has been taken into account using Equation (12). The combined standard uncertainty associated with each calorimetric measurement shown in Figure 6 was derived in accordance with ISO guidelines (ISO

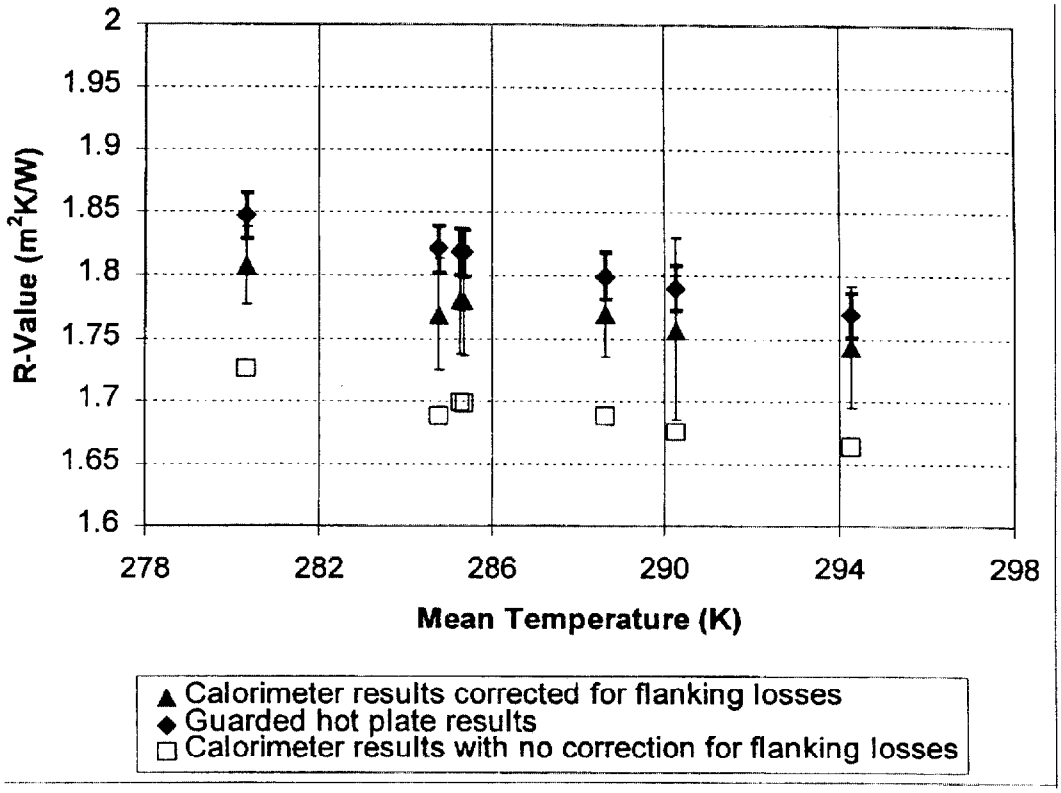

Figure 6. Comparison of calorimeter results to guarded hot plate results

1993). As indicated in Table 1, the combined standard uncertainty of the calorimeter ranges from 1.7% to 4.1% of the stated value. For a homogeneous panel, the uncertainty analysis takes into account the uncertainty associated with the power supplied to the heater, metering area, temperature measurements, surface conductances, and flanking loss.

The guarded hot plate results are shown as diamonds in Figure 6. The observed difference between the guarded hot plate and calorimeter results ranges from 1.8% to 3.0%. The standard uncertainty u_{OD} associated with the observed difference may be expressed as

$$u_{OD} = \sqrt{u_{GHP}^2 + u_{CF}^2} \tag{14}$$

where

u_{GHP} standard uncertainty associated with the guarded hot plate
u_{CF} standard uncertainty associated with the calorimetric facility

As shown in Table 1, the difference between the calorimetric and guarded hot plate results for six of the seven mean specimen temperatures is less than or equal to the uncertainty of the observed difference. The observed difference for the remaining point, Test G, is greater than the uncertainty of the observed difference.

For an inhomogeneous panel such as an advanced insulation panel, the uncertainty analysis must also consider the uncertainty associated with heat transfer through the mask. Uncertainties attributable to the flanking loss and mask heat transfer increase in significance as the panel R-value increases and as the panel size decreases. As an example, for an insulation panel with an

Table 1. Uncertainty Analysis Results

Test Identification	Mean Temperature (K)	Calorimeter Measurement Combined Standard Uncertainty (%)	Observed Difference (%)[1]	Uncertainty in Observed Difference (%)[2]
A	285.3	2.4	2.2	2.5
B	288.7	1.9	1.8	2.1
C	294.3	2.8	1.8	2.9
D	280.4	1.7	2.0	2.0
E	290.3	4.1	2.2	4.1
F	285.4	2.4	2.3	2.6
G	284.8	2.5	3.0	2.6

Notes:
1. Observed difference is defined as the difference between the calorimeter and guarded hot plate results as a percentage of the guarded hot plate results.
2. Uncertainty in observed difference is defined as the uncertainty in the difference between the calorimeter and guarded hot plate results as a percent of the guarded hot plate results.

R-value of 6 $m^2 \cdot K/W$, a temperature difference of 25 K, and an area equal to 70% of the total face area of the calorimeter, the uncertainty in the measured R-value is 4.4%. For an insulation panel with an R-value of 6 $m^2 \cdot K/W$, a temperature difference of 25 K, and an area equal to 40% of the total face area of the calorimeter, the uncertainty in the measured R-value is 11%.

CONCLUSIONS

The calorimeter apparatus described provides a practical and accurate means for determining the thermal resistance of advanced insulation panels. The technique for applying the calorimeter corrects for interactions between the mask and insulating panel and accounts for flanking loss through the perimeter of the mask. Finite element modeling was used to determine the flanking loss correction. For a specific calorimeter and mask construction, the resulting flanking loss correction can be correlated based on a linear function of the air temperature difference between the two sides of the mask. Using these techniques, measurements made using an extruded polystyrene panel were found to be within 3% of those obtained using a guarded hot plate apparatus.

ACKNOWLEDGEMENTS

The authors thank Stanley Morehouse for his assistance with the testing associated with the calorimeter; Robert Zarr and Paul Embree for providing the guarded hot plate measurements; Keith Eberhart for his guidance in calculating the measurement uncertainties; and Doug Burch for his valuable suggestions throughout this project.

NOMENCLATURE

A	area, m^2
h	surface conductance, $W/(m^2 \cdot K)$
k	thermal conductivity, $W/(m \cdot K)$
L	length, m
Q	heat transfer rate, W
R	thermal resistance, $m^2 \cdot K/W$
T	temperature, K
u	uncertainty, %

Subscripts

C	climatic chamber
CF	calorimetric facility
F	flanking
GHP	guarded hot plate
HTR	calorimeter heater
IP	insulating panel
M	mask or metering chamber
OD	observed difference
SC	panel surface exposed to climatic chamber
SM	panel surface exposed to metering chamber
W	metering chamber wall

REFERENCES

ASTM Standard C 177. 1997. Standard Test Method for Steady-State Heat Flux Measurements and Thermal Transmission Properties by Means of the Guarded-Hot-Plate Apparatus. *Annual Book of ASTM Standards*, 04.06: 20-41.

ASTM Standard C 236. 1997. Standard Test Method for Steady-State Thermal Performance of Building Assemblies by Means of a Guarded Hot Box. *Annual Book of ASTM Standards*, 04.06: 62-72.

ASTM Standard C 518. 1997. Standard Test Method for Steady-State Heat Flux Measurements and Thermal Transmission Properties by Means of the Heat Flow Meter Apparatus. *Annual Book of ASTM Standards*, 04.06: 160-162.

ASTM Standard C 976. 1997. Standard Test Method for Thermal Performance of Building Assemblies by Means of a Calibrated Hot Box. *Annual Book of ASTM Standards*, 04.06: 474-492.

Brandreth, D.A. 1991. Insulation Foam Aging—A Review of the Relevant Physical Phenomena. *Improved Thermal Insulation Problems and Perspectives*. New Holland, PA: Technomic Publishing Co.

Caps, R., Th. Rettelback, M. Ehrmanntraut, S. Korder, and J. Fricke. 1997. Development of Vacuum Super Insulations with Glass Cover and Powder Filling. *Insulation Materials: Testing and Applications: Third Volume*, ASTM STP 1320, R.S. Graves and R.R. Zarr, Eds., American Society for Testing and Materials.

Fanney, A.H., C.A. Saunders, and S.D. Hill. 1995. Test Procedures for Advanced Insulation Panels. *Proceedings of the BETEC Conference on Superinsulations and the Building Envelope*, 149-161.

Glicksman, L.R., N. Solomou, and J.K. Hong. 1995. Development of Rigid Foam/Evacuated Perlite Powder Composite Panels for Thermal Insulation. *Proceedings of the BETEC Conference on Superinsulations and the Building Envelope*, 29-51.

Griffith, B. and D. Arasteh. 1992. Gas-Filled Panels: A Thermally Improved Building Insulation. *Proceedings of the ASHRAE/DOE/BTECC Conference on the Thermal Performance of the Exterior Envelopes of Buildings – V*, 96-102.

ISO. 1993. Guide to the Expression of Uncertainty in Measurement, *International Organization for Standardization*, Geneva, Switzerland.

Lavine, A.G., J.L. Rucker, and K.E. Wilkes. 1981. Flanking Loss Calibration for a Calibrated Hot Box. *Proceedings of ASTM/DOE Conference on Thermal Insulation, Materials, and Systems for Energy Conservation in the '80s*, 234-247.

National Institute of Building Sciences (NIBS). 1995. *Proceedings of the BETEC Conference on Superinsulations and the Building Envelope.*

Zarr, R.R. and M.H. Hahn. 1996. Line Heat Source Guarded Hot Plate Apparatus: Adjunct ASTM Practice C 1043. *Annual Book of ASTM Standards*, 04.06: 525-528.